Eur. Phys. J. A (2019) **55**: 96
DOI 10.1140/epja/i2019-12775-5

THE EUROPEAN PHYSICAL JOURNAL A

Regular Article – Experimental Physics

Evaluation of high-precision atomic masses of A ∼ 50–80 and rare-earth nuclides measured with ISOLTRAP

W.J. Huang[1,2,a], D. Atanasov[3], G. Audi[1], K. Blaum[2], R.B. Cakirli[4], A. Herlert[5], M. Kowalska[3], S. Kreim[2,3], Yu.A. Litvinov[6], D. Lunney[1], V. Manea[1], M. Mougeot[1,2], M. Rosenbusch[7], L. Schweikhard[8], A. Welker[3], F. Wienholtz[8], R.N. Wolf[2,8,b], and K. Zuber[9]

[1] CSNSM-IN2P3/CNRS, Université Paris-Sud, 91405 Orsay, France
[2] Max-Planck-Institut für Kernphysik, Saupfercheckweg 1, 69117 Heidelberg, Germany
[3] CERN, 1211 Geneva 23, Switzerland
[4] University of Istanbul, Department of Physics 34134, Istanbul, Turkey
[5] FAIR GmbH, Planckstraße 1, 64291 Darmstadt, Germany
[6] GSI Helmholtzzentrum für Schwerionenforschung GmbH, Planckstraße 1, 64291 Darmstadt, Germany
[7] RIKEN Nishina Center, Wako, Saitama 351-0198, Japan
[8] Institut für Physik, Universität Greifswald, Felix-Hausdorff-Straße 6, 17489 Greifswald, Germany
[9] Institut für Kern- und Teilchenphysik, Technische Universität Dresden, 01069 Dresden, Germany

Received: 8 March 2019 / Revised: 8 May 2019
Published online: 21 June 2019

Communicated by A. Jokinen

Abstract. High-precision mass measurements of stable and beta-decaying nuclides $^{52-57}$Cr, ^{55}Mn, ^{56,59}Fe, ^{59}Co, $^{75,77-79}$Ga, and the lanthanide nuclides ^{140}Ce, ^{140}Nd, ^{160}Yb, ^{168}Lu, ^{178}Yb have been performed with the Penning-trap mass spectrometer ISOLTRAP at ISOLDE/CERN. The new data are entered into the Atomic Mass Evaluation and improve the accuracy of masses along the valley of stability, strengthening the so-called backbone. The mass of neutron-deficient ^{168}Lu in its isomeric state has been measured directly. The mass of neutron-rich ^{178}Yb indicates a change of nuclear structure approaching the double harmonic-oscillator shell closure for $Z = 70$ and $N = 112$.

1 Introduction

The mass reflects all the interactions at work in the nucleus through the nuclear binding energy [1]. Masses are important benchmarks for many nuclear models and can be measured either indirectly, via decays and reactions, or directly as mass doublets with respect to a well-known reference. Data from these different methods are combined within the Atomic Mass Evaluation (AME) [2] that employs a least-squares adjustment procedure of all input data and generates a table of atomic masses. The AME has provided this important source to the community for the past several decades and continues to do so within an international collaboration (see [3], and the references therein).

The masses of many nuclides, most of which are stable, have been determined to precisions better than 1 keV, forming the "backbone" of the Atomic Mass Evaluation. While γ-ray energy measurements following a neutron-capture reaction on a neighboring isotope have provided many of the highest precision mass data, it is direct mass measurements using Penning-trap mass spectrometry [4] that now routinely fulfill this role. Because of the many links, improved measurements of nuclides comprising the backbone also improve masses farther away from the valley of stability [2]. Examination of nuclear structure changes via the nuclear binding energy is done by taking derivatives, such as neutron (proton) separation energies, empirical shell gaps, or nucleon-pairing energies, all of which amplify the need for precise measurements. Masses are a unique characteristic of the nucleus and form a surface with astonishing regularity (see series of graphs in the AME [2]). Irregularities in the mass surface can indicate new nuclear structure effects or experimental mistakes. Therefore, it is important to certify that measurements are also accurate. This is best accomplished by using different methods. Since the AME integrates all available data, it gives important hints as to where potential problems might arise.

[a] e-mail: huang@mpi-hd.mpg.de
[b] *Present address:* ARC Centre for Engineered Quantum Systems, School of Physics, The University of Sydney, NSW 2006, Australia.

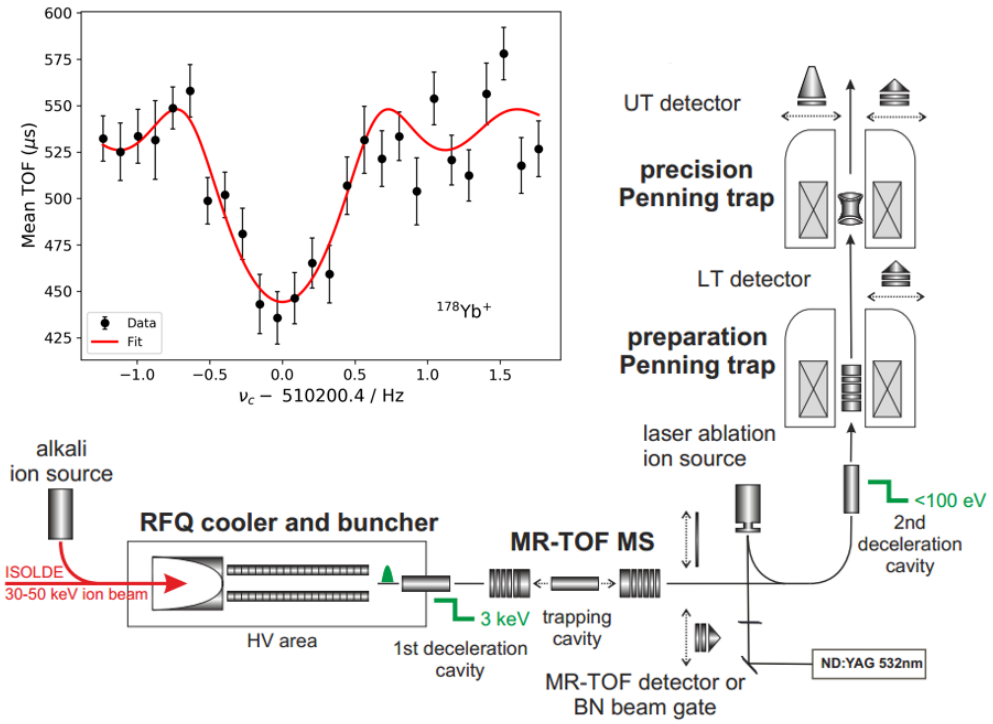

Fig. 1. Schematic view of the ISOLTRAP setup [11]. The insert shows a ToF-ICR spectrum for ^{178}Yb$^+$. See text for details.

In this paper, we present a series of measurements of stable and quasi-stable nuclides around $A = 55$, short-lived gallium isotopes and rare-earth nuclides ^{140}Ce, ^{140}Nd, ^{160}Yb, ^{168}Lu, ^{178}Yb. We describe their production and their mass measurement with the ISOLTRAP apparatus [5]. We introduce the new mass values into the Atomic Mass Evaluation (AME) and compare them to previously measured data. We also examine the new resulting mass surface and in particular discuss some nuclear structure for ^{178}Yb and the isomeric state of ^{168}Lu.

The method of choice for precision measurements is Penning-trap mass spectrometry [4]. The cyclotron frequency ν_c of an ion of interest is measured in a strong magnetic field, which relates directly to the mass of a nuclide:

$$\nu_c = \frac{1}{2\pi}\frac{q}{m}B, \qquad (1)$$

where q/m is the charge-to-mass ratio and B is the strength of the magnetic field. Penning traps have provided numerous precise mass-spectrometric data. For example, the mass of light, stable nuclides have been determined with relative uncertainties below $\delta m/m \sim 10^{-10}$ [6–8]. To calibrate the magnetic field, Penning-trap mass spectrometry compares the mass of an unknown nuclide with another reference nuclide (often, the easily ionizable alkali species) whose mass is well known. This also circumvents the possibility of propagating error along an isotopic chain as in the case of (n,γ) measurements or along isobaric chains in the case of β decay.

In the following, the experimental setup will be discussed in sect. 2 along with the data analysis and results will be discussed in sect. 3. The summary will be given in sect. 4.

2 Experimental setup

The Penning-trap mass spectrometer ISOLTRAP [5], installed at ISOLDE/CERN, aims primarily at accurate mass measurements of short-lived nuclides. Radioactive nuclides are produced by the bombardment of a thick, heated target with a 1.4-GeV proton beam from the CERN proton synchrotron booster (PSB). The resulting nuclides diffuse from the target material, pass through a transfer line and are ionized by different ionization techniques [9] such as surface ionization, laser ionization (Resonance Ionization Laser Ion Source RILIS), or plasma ionization, depending on the chemical properties of the nuclides under investigation. After ionization, the ions are accelerated and mass separated either by the High Resolution Separator (HRS) or General Purpose Separator (GPS) [10], with mass resolving powers of 5000 and 1000, respectively. The ion beam is then transported to the tandem Penning-trap mass spectrometer (see fig. 1).

The ISOLTRAP setup consists of four traps [11]: a linear radio-frequency quadrupole cooler and buncher (RFQ) [12], a multi-reflection time-of-flight mass separator/spectrometer (MR-ToF MS) [13], a cylindrical preparation Penning trap, and a hyperbolic precision Penning trap. The RFQ is placed on a voltage-floatable platform and is used for accumulating, cooling, and bunching the continuous ion beam of a transport energy of 30–50 keV delivered from ISOLDE. After a few milliseconds of accumulation, an ion bunch is ejected from the RFQ with a typical kinetic energy of $E_{trans} \approx 3$ keV and transferred to the MR-ToF MS. In the MR-ToF MS, the ions are trapped by use of the in-trap lift technique [14], which reduces the kinetic energy of the ions to $E_{trap} \approx 2$ keV.

Table 1. Experimental details for the production of the ions of interest. Listed are the experiment date, the target, the ionization technique, the ion energy of the ISOLDE beam, and the mass separator used.

Species	Date	Target	Ion source	Energy	Separator
^{168}Lu	Jun 2011	Ta	W surface	50 keV	GPS
^{178}Yb	Oct 2011	Ta	RILIS	30 keV	HRS
^{160}Yb, ^{140}CeO, ^{140}NdO, ^{156}Dy	Aug 2014	Ta	W surface	30 keV	GPS
$^{52,55-57}$Cr, ^{56,59}Fe	Oct-Nov 2014	UCx	Ta surface	30 keV	HRS
$^{75,77-79}$Ga	Jun 2015	UCx-n	Ta surface	30 keV	HRS
$^{52-54}$Cr, ^{55}Mn	Apr 2016	UCx	Ta surface/RILIS	30 keV	HRS

The contaminants can be separated after several hundred reflections between two electrostatic mirrors, based on different flight times due to mass-to-charge ratios. If the ion beam is strongly contaminated by isobars, one can use a Bradbury-Nielsen gate [15] or selected in-trap-lift ejection [16] to suppress the contaminants. Subsequently, the bunch is transferred upwards to the preparation Penning trap for further purification and cooling. Finally, the purified ions are transferred to the precision Penning trap for high-precision mass measurements.

The ions in a Penning trap perform three independent, harmonic eigenmotions [17]: the oscillation along the trap axis at the axial oscillation frequency ν_z, the cyclotron motion at the so-called modified cyclotron frequency ν_+, and the magnetron motion at frequency ν_-. The latter two motions are radial motions perpendicular to the trap axis. What interests us is the cyclotron frequency, see eq. (1), from which the mass of an unknown nuclide can be deduced. The determination of ν_c can be achieved by employing the time-of-flight ion-cyclotron-resonance (ToF-ICR) technique [18]. In the precision Penning trap, a dipole excitation is first applied at the ion's magnetron frequency, which brings the originally on-axis ions on a trajectory with a radius of about 0.7 mm. Then, a quadrupole rf excitation is applied for an excitation duration T_{rf}, which converts the magnetron motion to the modified cyclotron motion [19]. The conversion is resonant at the sum of the modified cyclotron frequency and the magnetron frequency which results in the cyclotron frequency of eq. (1), *i.e.* $\nu_c = \nu_+ + \nu_-$. After T_{rf}, the ions are extracted towards a timing detector (MCP) located outside of the strong magnetic field. To obtain the time-of-flight spectrum, the frequency of the rf field is scanned around the ion's cyclotron frequency. The time of flight of the ions from the center of the precision Penning trap to the MCP detector is recorded. The cyclotron frequency of the ions of interest is then determined by fitting the average time-of-flight values as a function of excitation frequency with the theoretical curve [19].

A ToF-ICR spectrum of ^{178}Yb is displayed in the insert of fig. 1, where the excitation duration was set to $T_{rf} = 1.2$ s. The x-axis denotes the quadrupole rf-excitation frequency and the y-axis represents the mean time of flight of the ions. The black points represent the experimental data and the red line is the theoretical resonance curve [19]. To calibrate the magnetic field, the cyclotron frequency $\nu_{c,ref}$ of an ion with well-known mass is measured before and after the measurement of the ion of interest. The cyclotron frequency of the reference ion is interpolated to the time when the ion of interest is measured. To improve the precision, the Ramsey-type ion-cyclotron excitation scheme [20,21] was also employed in some cases.

The mass measurements in this paper stem from several experimental campaigns which took place between 2011 and 2016, and made use of different targets and ionization techniques. The heavier, proton-rich rare-earth nuclides were produced by spallation of a tantalum target. In two cases (^{140}Ce and ^{140}Nd), the isotopes were released from the target as oxides. The lighter and neutron-rich species were produced from fission of a uranium carbide (UC_x) target, which was equipped with a neutron converter in the case of the gallium isotopes. The related information is listed in table 1.

Since all measurements involved singly-charged ions, the atomic mass m of the nuclide of interest is obtained from:

$$m = r \times (m_{ref} - m_e) + m_e, \quad \text{with } r = \frac{\nu_{c,ref}}{\nu_c}, \qquad (2)$$

where m_{ref} is the atomic mass of the reference nuclide and m_e is the electron mass. The atomic binding energy and the relativistic effect can be neglected at the level of precision of the present measurements. Apart from the statistical uncertainty, the mass-dependent shift and the short-term magnetic field fluctuation [22] were also taken into account. The systematic uncertainties were added in quadrature with the statistical uncertainties. In the analysis, the number of ions per shot was restrict to a maximum of five so the ion-ion interaction was minimized. The z-class analysis [22] was also carried out for two cases (^{59}Co and ^{160}Yb, due to their high production yield).

The cyclotron frequency ratios of the ions of interest and the corresponding reference ion are listed in table 2, along with the derived mass excess (ME) in keV. The fre-

Table 2. Frequency ratios of nuclides investigated. Listed are also the half-lives, the reference ion, the mass excess (ME) from ISOLTRAP and the 2012 Atomic Mass Evaluation (AME2012). The seventh column is the new adjustment after including the ISOLTRAP results. The eighth column is the discrepancy of the ISOLTRAP data with respect to the new adjusted results divided by the mass uncertainty of ISOLTRAP. The ninth column is the influence in percentage of each ISOLTRAP measurement. In case of oxides, the mass excess values were obtained by subtracting the known mass −4737.0014(2) keV of ^{16}O.

Nuclide	$T_{1/2}$	Ref.	$r = \frac{\nu_{c,ref}}{\nu}$	ME (keV)			sigma	Influence %
				ISOLTRAP	AME2012	AME2012+ISOLTRAP		
^{52}Cr[a]	Stable	^{39}K	1.3330530344(124)	−55419.7(4)	−55418.1(6)	−55419.69(24)	−0.02	30%
^{52}Cr		^{85}Rb	0.6116970566(67)	−55419.4(5)			0.58	21%
^{53}Cr	Stable	^{85}Rb	0.6234757106(68)	−55288.8(5)	−55285.9(6)	−55287.53(24)	−2.53	21%
^{54}Cr	Stable	^{85}Rb	0.6352318839(81)	−56936.4(6)	−56933.7(6)	−56935.29(25)	−1.84	16%
^{55}Cr[a,b,c]	3.497 m	^{85}Rb	0.6470319500(225)	−55112.3(18)	−55108.6(6)	−55110.24(32)	−1.14	0%
^{56}Cr[a]	5.94 m	^{56}Fe	1.0001021453(98)	−55284.4(7)	−55281.2(19)	−55285.06(58)	−0.94	100%
^{57}Cr[a,b,c]	21.1 s	^{85}Rb	0.6706186690(233)	−52525.0(18)	−52524.1(19)	−52524.56(13)	−0.24	50%
^{55}Mn[a]	Stable	^{85}Rb	0.6469990878(94)	−57711.5(7)	−57711.7(4)	−57712.47(27)	1.39	13%
^{56}Fe[a]	Stable	^{85}Rb	0.6587394873(71)	−60606.9(6)	−60606.4(4)	−60607.09(27)	0.32	23%
^{59}Fe[a]	44.495 d	^{85}Rb	0.6940697718(126)	−60664.1(10)	−60664.2(5)	−60664.89(33)	0.79	10%
^{59}Co	Stable	^{39}K	1.5125223446(390)	−62227.8(14)	−62229.1(5)	−62229.68(37)	1.34	7%
^{75}Ga[b]	126 s	^{85}Rb	0.8824032589(85)	−68460.6(7)	−68464.6(24)	−68460.6(7)	0	100%
^{77}Ga	13.2 s	^{85}Rb	0.9059884396(537)	−65995.0(42)	−65992.3(24)	−65992.3(24)	−0.6	0%
^{78}Ga	5.09 s	^{85}Rb	0.9177944088(139)	−63704.0(11)	−63706.0(19)	−63704.1(11)	0.09	88%
^{79}Ga	2.848 s	^{85}Rb	0.9295860176(201)	−62548.8(16)	−62547.7(19)	−62548.3(12)	−0.28	58%
^{140}Ce[a,d]	Stable	^{133}Cs	1.1730177964(188)	−88072.0(23)	−88079.2(22)	−88075.4(15)	1.49	44%
^{140}Nd[a,d]	3.34 d	^{133}Cs	1.1730486098(261)	−84257.3(32)	−84254(26)	−84257.3(33)	−0.03	100%
^{156}Dy[a]	Stable	^{133}Cs	1.1731978110(338)	−70523.1(42)	−70528.3(16)	−70528.79(12)	1.35	8%
^{160}Yb[a]	4.8 m	^{133}Cs	1.2033943563(443)	−58163.2(55)	−58165(16)	−58163.2(55)	0.0	100%
^{168m}Lu[e]	6.7 m	^{133}Cs	1.2635979084(465)	−56908.2(58)	−56870(39)	−56908.2(58)	0.0	100%
^{178}Yb	74 m	^{85}Rb	2.095672299(110)	−49663.1(87)	−49694(10)	−49677.1(66)	1.61	57%

[a] Already included in AME2016.
[b] Measured by the Ramsey method.
[c] Extra systematic error was added to account for liquid helium-filling close to the time of the measurement.
[d] Measured as oxides.
[e] Assigned to the $J^\pi = 3^+$ isomeric state.

quency ratios were included into the Atomic Mass Evaluation database and a global adjustment was performed. Since some of the present data has been included in the atomic mass table AME2016 [23], values from the mass table AME2012 [3] are given instead for comparison. The resulting influence of the new data is listed in the last column. These values range from 0% (still valuable for a consistency check) to 100% in five cases. The half-lives of all nuclides [24] are also listed. The results and their impact with respect to previous mass determinations are discussed in the following section. The differences between the mass excess (ME) values determined in this work and those in AME2012 are illustrated in fig. 2.

3 Results and discussion

3.1 The A = 52–59 region

The masses of $^{52-57}$Cr ($Z = 24$) were measured in two experimental campaigns in 2014 and 2016. The results show that the new masses of the chromium isotopes are systematically smaller than the values in AME2012 by 1–3 keV (see table 2 and fig. 2). There, the $^{52-55}$Cr masses were mainly determined by a series of (n, γ) reactions with precision better than 0.3 keV. A (p, γ) reaction [25] also determines the mass of ^{54}Cr by 42%. Other reactions contribute much less to the chromium mass region under discussion.

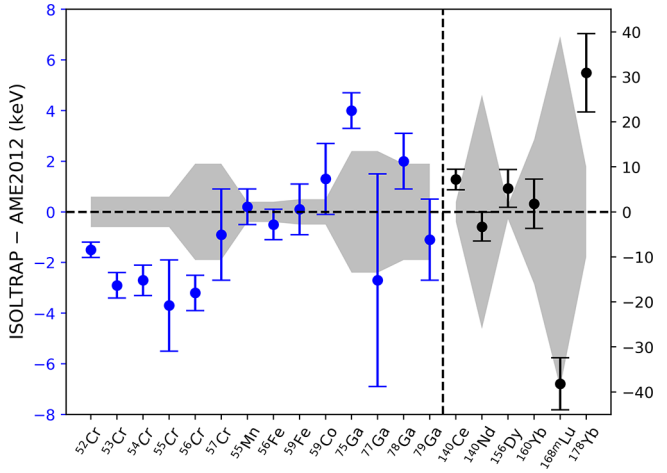

Fig. 2. Differences between the mass-excess values determined in this work and those from AME2012. Different scales on the y-axis are used to display differences in two mass regions separated by a vertical dashed line. The grey shadings indicate the AME2012 uncertainties (in the corresponding region).

The masses of ^{56}Cr and ^{57}Cr in AME2012 were determined uniquely by ISOLTRAP [26]. The new ISOLTRAP results differ from the previous ones by $-3.2(20)$ keV and $-0.9(26)$ keV, respectively. The results obtained from the current analysis agree well with the older results but the uncertainty of the mass of ^{56}Cr is improved by almost a factor of three.

Figure 3 displays a diagram of the flow of information in the chromium region, where the numbers in bold next to the arrows indicate the influences (in percentage) that flow into each mass and the numbers in the bottom-right corner of each box indicate the mass uncertainty. The numbers in black represent the evaluation result in AME2012 and the numbers in blue represent the new evaluation result.

After the global evaluation, we found that the mass uncertainties of $^{52-55}$Cr have been reduced by a factor of at least two, which largely strengthens the AME backbone. The new mass values of ^{52}Cr and ^{55}Cr agree with the adjusted masses within 1.5σ, while those of ^{53}Cr and ^{54}Cr differ from the adjusted values by $-1.3(5)$ keV and $-1.1(6)$ keV, respectively (see table 2). We can see from fig. 3 that the mass of ^{53}Cr is now determined by the mass links ^{52}Cr(n,γ) (47.1%), ^{53}Cr(n,γ) (32.2%), and the ISOLTRAP result (20.7%). The discrepancy originates from the mass difference between ^{52}Cr and ^{53}Cr. The Q-value for ^{52}Cr$(n,\gamma)^{53}$Cr is determined to be 7940.5(7) keV based on the ISOLTRAP results. However, this value is not consistent with the three input values 7939.5(3) keV [27], 7939.0(2) keV [28] and 7939.1(3) keV [29], which give the average value 7939.15(14) keV. The difference between the ISOLTRAP result and the average (n,γ) value is 1.4(7) keV, an acceptable discrepancy, requiring no reconsideration of the systematic error in our results.

Using the masses of ^{53}Cr and ^{54}Cr, the Q-value for the reaction ^{53}Cr$(n,\gamma)^{54}$Cr can be derived to be 9718.9(7) keV. In AME2012, this reaction Q-value was the average of four input values: 9719.3(2) keV [30], 9718.3(4) keV [31], 9718.9(3) keV [27], and 9719.7(5) keV [32], resulting in an average value of 9719.14(13) keV, which is in reasonable agreement with the ISOLTRAP result.

The mass of ^{53}Cr was measured in the same run as ^{52}Cr, ^{54}Cr, and ^{55}Mn. The latter three nuclides are in agreement with the global evaluation. The masses of $^{52-54}$Cr were recently measured to slightly better precision with the Penning trap facility LEBIT [33]. While the LEBIT value for ^{53}Cr of $-55287.5(2)$ keV differs from ISOLTRAP by about 2σ, it is about 3-sigma more bound than the AME2012 value. The LEBIT mass for ^{54}Cr is about 1.5σ from the ISOLTRAP result and the ^{52}Cr mass agrees to within 1σ.

The mass of ^{55}Mn was well-known in AME2012 with a precision of 0.4 keV. The resulting value from ISOLTRAP gave a mass excess of $-5711.5(7)$ keV, in agreement with the AME2012 adjusted value, and has an influence of 13% on the determination of ^{55}Mn.

The mass excess of ^{56}Fe was determined in AME2012 to be $-60606.4(4)$ keV through several links. The new direct value from ISOLTRAP yields $-60606.9(6)$ keV, which now contributes by 23%.

The mass of ^{59}Fe was determined to be $-60664.2(5)$ keV in AME2012 by the average of three (n,γ) reactions. Our measurement yields a value of $-60664.1(10)$ keV, which agrees nicely with the recommended value.

The AME2012 mass of ^{59}Co was determined through indirect reaction measurements, resulting in a mass excess of $-62229.1(5)$ keV. ISOLTRAP now provides a direct mass excess of $-62227.8(14)$ keV, in agreement with the recommended value in AME2012 and contributing 7%.

3.2 The gallium masses

The mass of ^{75}Ga was previously determined to be $-68464.6(24)$ keV by ISOLTRAP [34]. The newly determined mass gives a value of $-68460.6(7)$ keV, in agreement with the previous value but three times more precise.

The mass of ^{77}Ga was also determined uniquely in AME2012 by ISOLTRAP [34]. The new ISOLTRAP value is $-65995.0(42)$ keV, in agreement with the previous result of $-65992.4(24)$. The policy of the AME is to keep the most precise value provided by the same apparatus.

In AME2012, the mass of ^{78}Ga was determined to be $-63706.0(19)$ keV by averaging two Penning-trap results of $-63706.6(24)$ keV from ISOLTRAP [34] and $-63705(3)$ keV from JYFLTRAP [35]. The new measurement gives a value of $-63704.0(11)$ keV, which supercedes the previous ISOLTRAP value [34] and determines by 88% of the mass of ^{78}Ga in the new adjustment.

The AME2012 mass of ^{79}Ga was $-62547.7(19)$ keV from JYFLTRAP [35]. The new ISOLTRAP mass of $-62548.8(16)$ keV agrees and now contributes by 58%.

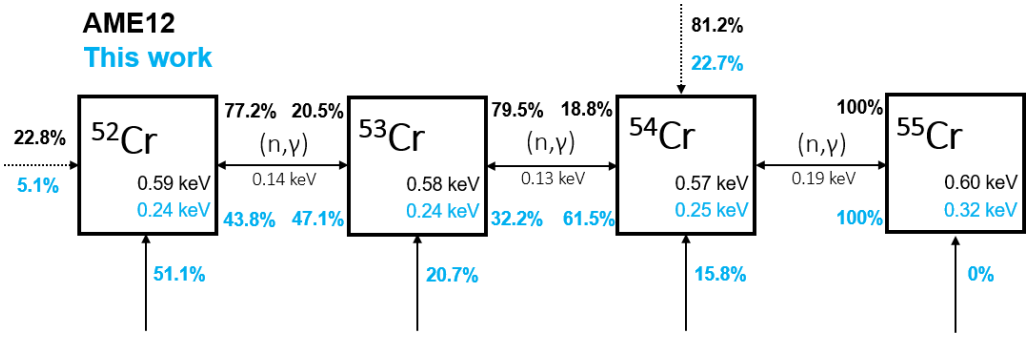

Fig. 3. Flow of information for the chromium masses from $A = 52$ to $A = 55$. Each box represents a nuclide, with the mass uncertainty (in keV) in the lower right corner. The numbers in black represent the former evaluation in AME2012, and numbers in blue represent the new evaluation including the new chromium results. The numbers in blue in the lower parts indicate the influences of the current data on the corresponding nuclides. The dashed arrows indicate the contribution from other experiments.

3.3 The lanthanide masses

In AME2012, the mass excess of ^{140}Ce was determined by different reaction measurements to be −88079.2(22) keV. ISOLTRAP gives a new mass value of −88072.0(23) keV with a comparable precision but differing from the AME2012 value by 7.2(32) keV. Including the ISOLTRAP result into the new adjustment shows that it differs from the adjusted value by 1.5σ.

The mass excess of ^{140}Nd is newly determined by ISOLTRAP to be −84257.3(32) keV. The ISOLTRAP result agrees with the previous measurement using storage-ring mass spectrometry (Schottky) at GSI [36] which provided an 87% contribution, while the rest was determined by ^{140}Pm$^m(\beta^+)^{140}$Nd [37] in AME2012. The ISOLTRAP result is eight times more precise and consequently outweighs all previous data.

The AME2012 mass of ^{156}Dy was mainly determined by Penning-trap spectrometry with SHIPTRAP [38]. The ISOLTRAP result agrees with their value within 1.4σ and provides an 8% contribution to the new adjusted value.

The mass excess −58165(16) keV of ^{160}Yb was provided uniquely in AME2012 by ISOLTRAP [39]. The new ISOLTRAP measurement yields a value of −58163.2(55) keV, in agreement with the AME2012 value but a factor of three more precise, hence replacing the older value.

3.3.1 Isomeric state assignment in ^{168}Lu

Two isomers were reported in ^{168}Lu [40] with half-lives of 5.5 minutes ($J^\pi = 6^-$) and 6.7 minutes ($J^\pi = 3^+$). In [40], the authors obtained two distinct β^+ spectra and the excitation energy for the higher isomeric state ($J^\pi = 3^+$) was determined to be 220(130) keV from two endpoint energies. The level scheme of ^{168}Lu was later re-investigated [41]. The intensity of a γ transition of 202.8 keV was determined to be 0.86(21) per 100 decays, which is much lower than the prediction [40]. The authors in [41] concluded that: "This transition is very weak in the γ channel: it was only observed in the total sum spectrum of all irradiations, so it was considered doubtful ..." No other transition from a low-spin state in the neighborhood of 220(130) keV was reported.

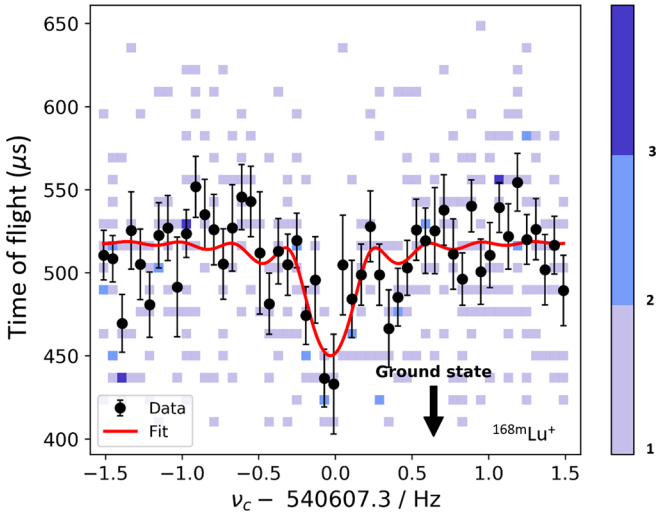

Fig. 4. Typical ToF-ICR resonance obtained for ^{168}Lu$^+$ with $T_{rf} = 1.2$ s. The 2D color map represents the number of ion events recorded in each (frequency,tof) bin. For each frequency bin, the mean time-of-flight and the associated standard deviation of the time-of-flight distribution is represented as black circles. The red line is a fit to the theoretical line shape [19]. The arrows indicate the position of the expected ground state.

The only direct mass measurement of ^{168}Lu was performed using Schottky mass spectrometry [36] at GSI and the mass value was assigned to the mixture of the ground and the isomeric state. In the current study, we looked for two states in ^{168}Lu. Figure 4 displays a 2D color map (ToF Matrix) which shows the ToF distribution (y-axis) recorded for each frequency steps of the frequency scan (x-axis). The color represents the number of events recorded in each of the 2D (frequency,tof) bins. Upon careful examination, the ToF matrix does not support the presence of excitation of the ions' cyclotron motion near the frequency expected for the ^{168}Lu$^+$ ground state. In another trial, we increased the excitation duration from 1.2 s

to 3 s but still only a single resonance was found. Based on the production yield study performed previously with ISOLTRAP [42], where ^{168}Lu was produced by the same reaction mechanism and the isomeric state of ^{168}Lu was populated 20 times more than the ground state, we are convinced that only the isomeric state was produced in the present experiments.

The new mass excess of the ^{168}Lu $J^\pi = 3^+$ isomeric state was determined to be $-56908.2(58)$ keV, in agreement with the recommended value in AME2012 but the precision has been improved by a factor of three. Combining our result with the recommended value of the ground state in AME2012 yields an excitation energy of 160(40) keV for the isomeric state, which is compatible with the excitation energy of 220(130) keV deduced from older endpoint energies [40], as already mentioned above.

3.3.2 Deformation of ^{178}Yb near the $N = 104$ midshell

The connection between the evolution of nuclear structure and experimental quantities has been widely discussed in different mass regions (see for example [43]). The illustrations and various observables of spectroscopic data, such as the ratio of $R_{4/2} \equiv E(4_1^+)/E(2_1^+)$, where $E(4_1^+)$ and $E(2_1^+)$ are the excitation energies of the first 4^+ and 2^+ states, respectively, and two-neutron separation energies, S_{2n}, are two straightforward ways to reveal the behavior of nuclear structure as a function of proton and neutron number. For example, as more neutrons are added to stable nuclides, a sudden increase of S_{2n} at $N \sim 90$ in $_{60}$Nd, $_{62}$Sm, and $_{64}$Gd signals the spherical-to-deformed transition region [44]. This transition can also be identified by a striking change of $R_{4/2}$ ratios in these three isotopic chains (see for example fig. 3 of [45]).

^{178}Yb ($Z = 70$) is the most neutron-rich nuclide with known mass in its isotopic chain. Its mass had been determined to be $-49694(10)$ keV from a ^{176}Yb(t, p) reaction [46]. The ISOLTRAP measurements give a result of $-49663.1(87)$ keV, which differs from the reaction value by 31(13) keV. Figure 5 displays the experimental two-neutron separation energies in the ytterbium region. For isotopic chains Hf ($Z = 72$), Ta ($Z = 73$), and W ($Z = 74$), the regular behavior of S_{2n} changes after crossing $N = 108$, where the linear trend is represented by a dashed line for each isotopic chain. This sudden drop of S_{2n} after crossing $N = 108$ was interpreted in terms of an energy gap above the Nilsson single-particle level $\frac{9}{2}^+[624]$ [47].

The S_{2n} value for ^{178}Yb is plotted by using the new ISOLTRAP result (represented by a red symbol). Even though the new ISOLTRAP result for ^{178}Yb differs from the reaction value [46] by 31(13) keV, an extra binding energy of ~ 440 keV is confirmed with respect to the regular trend. Unfortunately, the measurement of ^{179}Yb was not successful due to its low production rate. ^{176}Tm ($Z = 69$) is the last known nuclide of thulium and its mass came from a β^- decay [48] with a poor precision of 100 keV. The S_{2n} at $^{176}_{69}$Tm decreases significantly compared to other

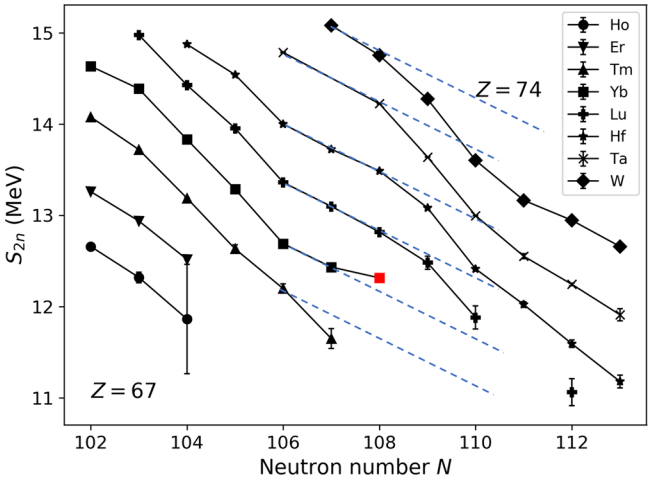

Fig. 5. Experimental two-neutron separation energies in the ytterbium region between Ho ($Z = 67$) and W ($Z = 74$). The red symbol is plotted using the new ^{178}Yb mass from ISOLTRAP. Dashed lines represent expected linear trends.

nuclides at $N = 107$. It has been suggested [49] that the even-even isotopes of Yb and Hf near $N = 104$ may manifest an SU(3) symmetry of the interacting boson model (IBM). The Hartree-Fock-Bogoliubov mass model HFB-27 predicts the mass of ^{178}Yb to be -49.61 MeV [50], which agrees with the present ISOLTRAP result. In the lower Z region, neither mass information nor spectroscopic data is available above $N = 105$. To clarify if a phase transition, *e.g.* from prolate to oblate, might occur in the ytterbium region at $N = 108$, mass measurements of ^{179}Yb, ^{180}Yb, and nuclides with $Z \leq 69$, $N \geq 105$ would be of great interest.

4 Summary

The masses of 20 stable and short-lived nuclides have been measured by the Penning-trap mass spectrometer ISOLTRAP with precisions of a few keV. Inclusion of the ISOLTRAP results into the global AME mass evaluation significantly reduced the uncertainties and strengthened the backbone of nuclides along the valley of stability. The mass of ^{168}Lu in its $J^\pi = 3^+$ isomeric state has been measured directly and the deduced excitation energy for the isomeric states is in agreement with the end-point energy measurement [40]. The new mass value of ^{53}Cr differs from the new evaluated result by 2.5σ, and the origin of the discrepancy was traced to the conflicting results between the indirect (n, γ) reactions and the direct ISOLTRAP results. A similar discrepancy is observed in results from LEBIT [33]. The mass measurement of ^{178}Yb confirms a gain in binding energy of ~ 440 keV with respect to the regular trend of the mass surface, which can be considered as a hint for structural change.

Open access funding provided by Max Planck Society. We thank the ISOLDE technical group and the ISOLDE Collaboration for their support. AW acknowledges support from the

Wolfgang Gentner program. RBC acknowledges support from the Max-Planck Partner group. WJH acknowledges the support from the China Scholarship Council (No. 201404910496). We acknowledge support by the French Institut National de Physique Nucléaire et de Physique des Particules (IN2P3), the Bundesministerium für Bildung und Forschung (05P12HGCI1, 05P12HGFNE, 05P15HGCIA, 05P15RDFN1, 05P15ODCIA), and the Max-Planck Society. This project has received funding through the European Union's Seventh Framework Programme for Research and Technological Development under Grant Agreements: 267194 (COFUND) and from the European Union's Horizon 2020 research and innovation programme under Grant Agreement No. 654002 and No. 682841. This project has also received funding from the European Union's Seventh framework through European Nuclear Science and Applications Research under Grant Agreement No. 262010.

Data Availability Statement This manuscript has no associated data or the data will not be deposited. [Authors' comment: The data are available on request.]

Publisher's Note The EPJ Publishers remain neutral with regard to jurisdictional claims in published maps and institutional affiliations.

References

1. D. Lunney, J.M. Pearson, C. Thibault, Rev. Mod. Phys. **75**, 1021 (2003).
2. W.J. Huang, G. Audi, M. Wang, F.G. Kondev, S. Naimi, X. Xu, Chin. Phys. C **41**, 030002 (2017).
3. M. Wang, G. Audi, A.H. Wapstra, F.G. Kondev, M. MacCormick, X. Xu, B. Pfeiffer, Chin. Phys. C **36**, 1603 (2012).
4. K. Blaum, Phys. Rep. **425**, 1 (2006).
5. M. Mukherjee, D. Beck, K. Blaum, G. Bollen, J. Dilling, S. George, F. Herfurth, A. Herlert, A. Kellerbauer, H.-J. Kluge, S. Schwarz, L. Schweikhard, C. Yazidjian, Eur. Phys. J. A **35**, 1 (2008).
6. F. DiFilippo, V. Natarajan, M. Bradley, F. Palmer, D.E. Pritchard, Phys. Scr. T **59**, 144 (1995).
7. M.P. Bradley, J.V. Porto, S. Rainville, J.K. Thompson, D.E. Pritchard, Phys. Rev. Lett. **83**, 4510 (1999).
8. B.J. Mount, M. Redshaw, E.G. Myers, Phys. Rev. A **82**, 5 (2010).
9. U. Köster, Eur. Phys. J. A **15**, 255 (2002).
10. R. Catherall, W. Andreazza, M. Breitenfeldt, A. Dorsival, G.J. Focker, T.P. Gharsa, Giles T.J., J.-L. Grenard, F. Locci, P. Martins, S. Marzari, J. Schipper, A. Shornikov, T. Stora, J. Phys. G **44**, 094002 (2017).
11. S. Kreim, D. Atanasov, D. Beck, K. Blaum, Ch. Böhm, Ch. Borgmann, M. Breitenfeldt, T.E. Cocolios, D. Fink, S. George, A. Herlert, A. Kellerbauer, U. Köster, M. Kowalska, D. Lunney, V. Manea, E. Minaya Ramirez, S. Naimi, D. Neidherr, T. Nicol, R.E. Rossel, M. Rosenbusch, L. Schweikhard, J. Stanja, F. Wienholtz, R.N. Wolf, K. Zuber, Nucl. Instrum. Methods Phys. Res. Sect. B **317**, 492 (2013).
12. F. Herfurth, J. Dilling, A. Kellerbauer, G. Bollen, S. Henry, H.-J. Kluge, E. Lamour, D. Lunney, R.B. Moore, C. Scheidenberger, S. Schwarz, G. Sikler, J. Szerypo, Nucl. Instrum. Methods Phys. Res. Sect. A **469**, 254 (2012).
13. R.N. Wolf, F. Wienholtz, D. Atanasov, D. Beck, K. Blaum, Ch. Borgmann, F. Herfurth, M. Kowalska, S. Kreim, Yu.A. Litvinov, D. Lunney, V. Manea, D. Neidherr, M. Rosenbusch, L. Schweikhard, J. Stanja, K. Zuber, Int. J. Mass Spectrom. **349**, 123 (2013).
14. R.N. Wolf, G. Marx, M. Rosenbusch, L. Schweikhard, Int. J. Mass Spectrom. **313**, 8 (2012).
15. N.E. Bradbury, R.A. Nielsen, Phys. Rev. **49**, 388 (1936).
16. F. Wienholtz, S. Kreim, M. Rosenbusch, L. Schweikhard, R.N. Wolf, Int. J. Mass Spectrom. **421**, 285 (2017).
17. L.S. Brown, G. Gabrielse, Rev. Mod. Phys. **58**, 233 (1986).
18. G. Gräff, H. Kalinowsky, J. Traut, Z. Phys. A **297**, 35 (1980).
19. M. König, G. Bollen, H.-J. Kluge, T. Otto, J. Szerypo, Int. J. Mass Spectrom. Ion Processes **142**, 95 (1995).
20. S. George, S. Baruah, B. Blank, K. Blaum, M. Breitenfeldt, U. Hager, F. Herfurth, A. Herlert, A. Kellerbauer, H.-J. Kluge, M. Kretzschmar, D. Lunney, R. Savreux, S. Schwarz, L. Schweikhard, C. Yazidjian, Phys. Rev. Lett. **98**, 162501 (2007).
21. S. George, K. Blaum, F. Herfurth, A. Herlert, Kretzschmar, S. Nagy, S. Schwarz, L. Schweikhard, C. Yazidjian, Int. J. Mass Spectrom. **264**, 110 (2007).
22. A. Kellerbauer, K. Blaum, G. Bollen, F. Herfurth, H.-J. Kluge, M. Kuckein, E. Sauvan, C. Scheidenberger, C.L. Schweikhard, Eur. Phys. J. D **22**, 53 (2003).
23. M. Wang, G. Audi, F.G. Kondev, W.J. Huang, S. Naimi, X. Xu, Chin. Phys. C **41**, 030003 (2017).
24. G. Audi, F.G. Kondev, M. Wang, W.J. Huang, S. Naimi, Chin. Phys. C **41**, 030001 (2017).
25. T. Weckström, Phys. Scr. **18**, 275 (1978).
26. C. Guénaut, G. Audi, D. Beck, K. Blaum, G. Bollen, P. Delahaye, F. Herfurth, A. Kellerbauer, H.-J. Kluge, D. Lunney, S. Schwarz, L. Schweikhard, C. Yazidjian, J. Phys. G **31**, S1765 (2005).
27. M.A. Islam, T.J. Kennett, S.A. Kerr, W.V. Prestwich, Can. J. Phys. **58**, 168 (1980).
28. J. Kopecky, R.E. Chrien, H.I. Liou, Nucl. Phys. A **334**, 35 (1980).
29. International Atomic Energy Agency, *Database of Prompt Gamma Rays from Slow Neutron Capture for Elemental Analysis* (IAEA, Vienna, 2007) `http://www-pub.iaea.org/books/IAEABooks/7030/Database-of-Prompt-Gamma-Rays-from-Slow-Neutron-Capture-for-Elemental-Analysis`.
30. D.H. White, D.J. Groves, R.E. Birkett, Nucl. Instrum. Methods **66**, 70 (1968).
31. G.D. Loper, G.E. Thomas, Nucl. Instrum. Methods **105**, 453 (1972).
32. C. Hofmeyr, Nucl. Phys. A **500**, 111 (1989).
33. R.M.E.B. Kandegedara, G. Bollen, M. Eibach, N.D. Gamage, K. Gulyuz, C. Izzo, M. Redshaw, R. Ringle, R. Sandler, A.A. Valverde, Phys. Rev. C **96**, 044321 (2017).

34. C. Guénaut, G. Audi, D. Beck, K. Blaum, G. Bollen, P. Delahaye, F. Herfurth, A. Kellerbauer, H.-J. Kluge, J. Libert, D. Lunney, S. Schwarz, L. Schweikhard, C. Yazidjian, Phys. Rev. C **75**, 044303 (2007).
35. J. Hakala, S. Rahaman, V.-V. Elomaa, T. Eronen, U. Hager, A. Jokinen, A. Kankainen, I.D. Moore, H. Penttilä, S. RintaAntila, J. Rissanen, A. Saastamoinen, T. Sonoda, C. Weber, J. Äystö, Phys. Rev. Lett. **101**, 052502 (2008).
36. Yu.A. Litvinov, H. Geissel, T. Radon, F. Attallah, G. Audi, K. Beckert, F. Bosch, M. Falch, B. Franzke, M. Hausmann, M. Hellström, Th. Kerscher, O. Klepper, H.-J. Kluge, C. Kozhuharov, K.E.G. Löbner, G. Münzenberg, F. Nolden, Yu.N. Novikov, W. Quint, Z. Patyk, H. Reich, C. Scheidenberger, B. Schlitt, M. Steck, K. Sümmerer, L. Vermeeren, M. Winkler, Th. Winkler, H. Wollnik, Nucl. Phys. A **756**, 3 (2005).
37. G.G. Kennedy, S.C. Gujrathi, S.K. Mark, Z. Phys. A **274**, 233 (1975).
38. S. Eliseev, M. Goncharov, K. Blaum, M. Block, C. Droese, F. Herfurth, E. Minaya Ramirez, Yu.N. Novikov, L. Schweikhard, V.M. Shabaev, I.I. Tupitsyn, K. Zuber, N.A. Zubova, Phys. Rev. C **84**, 012501 (2011).
39. G. Bollen, F. Ames, G. Audi, D. Beck, J. Dilling, O. Engels, S. Henry, F. Herfurth, A. Kellerbauer, H.-J. Kluge, A. Kohl, E. Lamour, D. Lunney, R.B. Moore, M. Oinonen, C. Scheidenberger, S. Schwarz, G. Sikler, J. Szerypo, C. Weber, Hyperfine Interact. **132**, 213 (2001).
40. A. Charvet, R. Chéry, D.H. Phuoc, R. Duffait, A. Emsalle, G. Marguier, Nucl. Phys. A **197**, 490 (1972).
41. V. Barci, G. Ardisson, D. Trubert, M. Hussonnois, Phys. Rev. C **55**, 2279 (1997).
42. D. Beck, F. Ames, G. Audi, G. Bollen, F. Herfurth, H.-J. Kluge, A. Kohl, M. König, D. Lunney, I. Martel, R.B. Moore, H. Raimbault-Hartmann, E. Schark, S. Schwarz, M. de Saint Simon, J. Szerypo, Eur. Phys. J. A **8**, 307 (2000).
43. R.B. Cakirli, R.F. Casten, Phys. Rev. C **78**, 041301(R) (2008).
44. A.E.L. Dieperink, O. Scholten, F. Iachello, Phys. Rev. Lett. **44**, 1747 (1980).
45. R.F. Casten, D.D. Warner, D.S. Brenner, R.L. Gill, Phys. Rev. Lett. **47**, 1433 (1981).
46. J.D. Zumbro, C.P. Browne, J.F. Mateja, H.T. Fortune, R. Middleton, Phys. Rev. C **26**, 965 (1982).
47. R.C. Barber, J.O. Meredith, F.C.G. Southon, P. Williams, J.W. Barnard, K. Sharma, H.E. Duckworth, Phys. Rev. Lett. **31**, 728 (1973).
48. S.C. Gujrathi, S.K. Mukherjee, Indian J. Phys. **41**, 633 (1967).
49. R.F. Casten, P. von Brentano, A.M.I. Haque, Phys. Rev. C **31**, 1991(R) (1985).
50. S. Goriely, N. Chamel, J.M. Pearson, Phys. Rev. C **88**, 061302 (2013).